Visualization and Tracking of Single Protein Molecules in the Cell Nucleus

Thorsten Kues, Reiner Peters, and Ulrich Kubitscheck
Institut für Medizinische Physik und Biophysik, Westfälische Wilhelms-Universität, D-48149 Münster, Germany

ABSTRACT A recently developed laser fluorescence videomicroscopy method was used to determine for the first time the intranuclear trajectories of single protein molecules. Using the recombinant *Escherichia coli* β-galactosidase protein P4K, labeled with an average of 4.6 ALEXA 488 chromophores per tetramer, single P4K molecules could be localized and tracked in the nuclei of permeabilized 3T3 cells at a spatial accuracy of ~30 nm and a time resolution of 18 ms. Our previous photobleaching measurements indicated that P4K had two fractions inside the nucleus, a larger mobile and a smaller immobile fraction. The present study supported this observation but revealed a much larger variety of mobility classes. Thus, a fraction of P4K molecules appeared to be truly immobile while another fraction was mobile but confined to very small areas. In addition, a large fraction of the P4K molecules appeared to be mobile and to move over extended distances by diffusion. However, a quantitative analysis showed that at least two subpopulations were present differing widely in diffusion coefficients. Importantly, both the diffusion coefficients and the fractions of these subpopulations were time-dependent. Our results suggest that proteins can move inside the nucleus over extended distances by diffusion. However, intranuclear protein diffusion is severely restricted, most likely by multiple association-dissociation events and/or impermeable obstacles.

INTRODUCTION

In the last few years the cell nucleus has been disclosed as a highly organized and compartmentalized structure. Chromosomes occupy distinct nuclear territories, which are probably further partitioned into distinct subcompartments (Manuelidis, 1990; Zhao et al., 1995; Dietzel et al., 1998). DNA transcription, replication and repair, and pre-mRNA splicing are performed by supramolecular structures that can be visualized as punctuate patterns, speckles, or foci of nuclear antigens by immunofluorescence studies (reviewed by Lamond and Earnshaw, 1998). Comprehending the principles that govern the architecture of chromosome territories, and their impact on the synthesis, processing, assembly, and transport of nuclear molecules and machines, is a major focus of current cell biological research.

One view to nuclear dynamics is obtained by studying the mobility of chromosomal structures. In general, two types of techniques were used for fluorescence labeling of single chromosomes or chromosomal loci in nuclei of living cells. One uses proteins that bind specifically to chromosomal subregions, and requires microinjection of the respective labeled proteins or antibodies, or the use of fusion proteins composing the green fluorescent protein. The other technique involves direct labeling of DNA by incorporating fluorophore-labeled nucleotide analogs during replication. Studies using these or related approaches detected various types of chromosomal, respectively centromeric movements (Shelby et al., 1996; Buchenau et al., 1997; Marshall et al., 1997; Abney et al., 1997; Zink et al., 1998). The emerging picture is that chromosomal motions are generally of Brownian type, but restricted to small nuclear subvolumes, and large-scale movements are relatively slow, selective, and infrequent (Zink and Cremer, 1998).

A complementary view of the intranuclear mobility arises if not only the dynamics of chromatin itself, but also the dynamics of molecules moving within these structures are examined (reviewed by Pederson, 2000). In this way the effects of existing structural domains and their constraints onto the transport properties inside the nuclear volume become visible. Such information was obtained by fluorescence microphotolysis methods (abbreviated as FM, FRAP, or FPR; Peters et al., 1974; Jacobson et al., 1976; Edidin et al., 1976; Axelrod et al., 1976; for review, see Peters and Scholz, 1991) and fluorescence correlation spectroscopy (FCS; Elson and Magde, 1974; Meseth et al., 1999).

Both FM and FCS have repeatedly been applied to the analysis of intranuclear mobility of a variety of probes. Inert tracer probes such as fluorescently labeled dextrans displayed apparent intranuclear diffusion coefficients that were approximately inversely proportional to the molecular radius, and appeared largely to be determined by viscosity and, to a smaller extent, by steric restriction effects (Peters, 1986; Lang et al., 1986; Seksek et al., 1997). The viscosity was found to be 4- to 10-fold higher than in dilute buffer solutions. For molecules with Stokes radii ranging from 2.2 to 30 nm no dependence of the ratio of intranuclear and aqueous diffusion coefficients on solute size was found. Fluorescent R-phycoerythrin (R-PE) was largely mobile (mobile fraction $f_{mob} = 93 \pm 4\%$) with an apparent intranuclear diffusion coefficient of $D_n = 4.4 \pm 1.3\ \mu m^2/s$, and appeared therefore to diffuse 10-fold slower than in buffer solution (Schulz and Peters, 1987; Wedekind et al., 1996).

Received for publication 22 November 1999 and in final form 28 February 2001.

Address reprint requests to Dr. Ulrich Kubitscheck, Institut für Medizinische Physik und Biophysik, Robert-Koch-Strasse 31, D-48149 Münster, Germany. Tel.: 251-83-56932; Fax: 251-83-55121; E-mail: kubitsc@uni-muenster.de.

0006-3495/01/06/2954/14 $2.00

Fluorescein-labeled nucleoplasmin, although of smaller size than R-PE, shows a smaller apparent intranuclear diffusion coefficient ($D_n = 2 \pm 0.8\ \mu m^2/s$). This observation was interpreted as formation of larger homo or heteropolymers, or weak interaction with intranuclear structures. In contrast to the latter probe molecules, fluorescently labeled BSA was largely immobile in the nucleus (Lang et al., 1986). A recombinant protein comprising the nuclear localization sequence (NLS) of the Simian virus (SV) 40 T-antigen and the almost complete β-galactosidase moiety (designated as P4K) was largely mobile ($f_{mob} = 68 \pm 10\%$), and displayed an apparent intranuclear diffusion coefficient of $D_n = 0.7 \pm 0.2\ \mu m^2/s$ in nuclei of polykaryons of rat hepatoma tissue culture cells (Rihs and Peters; 1989). This diffusion coefficient is >30-fold smaller than the theoretically expected diffusion coefficient in aqueous solution ($D_w = 33 \pm 3\ \mu m^2/s$). Diffusion nearly as rapid as in aqueous solution was observed for small oligodeoxynucleotides (Politz et al., 1998). Mobility of these probes was shown to be dependent on the hybridization state of the oligodeoxynucleotides. In a recent study Phair and Misteli used FRAP and fluorescence loss in photobleaching (FLIP) to observe the intranuclear movement of three proteins—the nucleosome-binding protein HMG-17, fibrillarin, and the pre-mRNA splicing factor SF2/ASF—in HeLa and BHK cells (Phair and Misteli, 2000). Each of these proteins was fused to the green fluorescent protein (GFP), and Phair and Misteli observed diffusion coefficients of 0.25–0.5 $\mu m^2/s$ for the three fusion proteins. These values were ~100-fold lower than those obtained for the respective molecules in buffer solutions. The significant reductions in free mobility were interpreted as indicating extensive association and dissociation of the examined proteins with intranuclear structures.

Single molecule detection in combination with single particle tracking is a novel approach to molecular transport investigations (SPT, for review see Saxton and Jacobson, 1997; Nie and Zare, 1997; Weiss, 1999; Mehta et al., 1999; Ishii and Yanagida, 2000). SPT has the major advantage of allowing the detection of distinct mobility modes in heterogeneous systems, where ensemble measurements would only yield an inhomogeneous broadening (Cherry, 1993). The detection of single molecules can be carried out by normal, far-field optical microscopy in combination with high-sensitivity video systems with a spatial accuracy below 50 nm and a time resolution in the millisecond range (Schmidt et al., 1995, 1996). If submicroscopic particles are imaged they appear as diffraction-limited spots, so-called Airy disks, of ~200 nm radius at a wavelength of 488 nm and a numerical aperture of 1.4. Although the shape of a submicroscopic particle cannot be resolved, the position of the particle center can be determined with very high precision by application of image processing and special fitting procedures. The accuracy of particle localization depends on the signal-to-noise ratio (SNR; Bobroff, 1986) and, according to previous studies (Kubitscheck et al., 1996, 1999) may amount up to 10 nm in *x*-, *y*-, and *z*-directions under optimal conditions.

Obviously, background reduction is the prerequisite of the optical detection of single fluorophores. Background fluorescence mainly arises from autofluorescence, out-of-focus fluorescence, and impurity fluorescence (Nie and Zare, 1997; Xie and Trautman, 1998). Therefore, in the past the reduction of the probed volume was a major means for reducing background fluorescence and improving the SNR. Reduction of the probed volume has been achieved by using particular optical techniques such as total internal reflection, near-field illumination, and multiphoton and confocal imaging. In cell biology SPT studies focused on membrane-bound fluorophores and their dynamics (reviewed by Saxton and Jacobson, 1997). Such studies allowed distinguishing various modes of receptor mobility, i.e., directed motion, anomalous or free diffusion, and to relate the mobility to structural features of the membrane.

Recently we showed that single protein molecules can also be visualized and tracked in extended three-dimensional (3D) samples with high precision (Kubitscheck et al., 2000). By using a wide-field fluorescence microscope equipped with a powerful light source and a low-light level CCD camera, single molecules of the GFP were detected in gels and viscous solutions at depths of up to ~10 μm from the interface. A high-speed framing mode accomplished a time resolution of 5 ms, allowing a two-dimensional (2D) localization of single molecules with an accuracy of ~30 nm. From the trajectories, diffusion coefficients of single GFP molecules were derived that were consistent with FM and other measurements.

In the present study we extended the technique to visualizing and tracking of single molecules in cell nuclei. A large tracer protein molecule was selected for a variety of reasons. The tracer should be large enough to carry several fluorophores, homogeneous in size, hydrophil, and inert in the nucleus. According to these conditions the above-mentioned hybrid protein P4K comprising the NLS of the SV40 large T-antigen and the complete β-galactosidase moiety was chosen (Rihs and Peters, 1989; Rihs et al., 1991), and labeled with ALEXA-488. We introduced the probe molecules into nuclei of digitonin-permeabilized cells by transport via the nuclear pore complex (NPC). The cytosol was substituted by an oocyte lysate supplemented by ATP, and an ATP regenerating system. The cytoplasmic extract contributed the various factors required for a transport of large proteins into the nucleus (Mattaj and Englmeier, 1998). This system (Adam et al., 1990) has been widely used in nucleocytoplasmic transport studies. After import of the ALEXA-labeled P4K single protein trajectories could be observed in the cell nuclei with a time resolution of 10 ms and with a lateral localization accuracy of ~35 nm.

MATERIALS AND METHODS

Proteins

The protein P4K in which the T antigen residues 111–135 are fused to the amino-terminus of *Escherichia coli* β-galactosidase was expressed in *E. coli* and purified by affinity chromatography as described (Rihs and Peters, 1989). P4K was transferred to 50 mM bicine/KOH (pH 7.8), 150 mM NaCl, and adjusted to 10 mg/ml (80 μM). The stock solution was stored in 50-μl aliquots at −80°C. According to x-ray analysis the β-galactosidase tetramer has a size of 17.5 × 13.5 × 9 nm^3 (Jacobson et al., 1994). This should result in an approximate diffusion coefficient of $D = 33 \pm 3\ \mu m^2/s$ in aqueous solution (Berg, 1983). Texas-Red-labeled 70-kDa dextran (TR-dextran) and ALEXA Fluor-488-labeled IgG were purchased from Molecular Probes, Inc. (Leiden, The Netherlands) and human serum albumin (HSA) was purchased from Sigma (Deisenhofen, Germany).

Labeling of P4K with ALEXA-488

An aliquot of the P4K stock solution (50 μl) was complemented with dithiothreitol (DTT, final concentration of 5 mM) and incubated for 1 h at 37°C. The reduced P4K was washed twice by dilution with 450 μl of 50 mM bicine/KOH (pH 7.8) and reconcentrated to 50 μl, using a centricon 100 cell (15 min, 4°C, 1000 × *g*). A 20-fold molar excess of 1 mM ALEXA Fluor-488 maleimide, sodium salt (ALEXA-488) in DMSO was added. The mixture was incubated for 2 h at room temperature in the dark. Finally, the reaction mixture was passed over a Sephadex-G25 column. The column was eluted with "transport buffer" (50 mM Hepes/KOH, pH 7.3, 110 mM potassium acetate, 5 mM sodium acetate, 2 mM magnesium acetate, 1 mM EGTA, 2 mM DTT). Fractions of ~700 μl were collected and checked for protein. Fractions containing protein were pooled and concentrated by centrifugation in a centricon 100 cell at 4°C and 1000 × *g*. Finally, the protein concentration was adjusted to 1 mg/ml. The protein was stored in small aliquots at −80°C. Similarly to P4K, HSA was labeled with ALEXA-488. In this preparation, however, an equimolar amount of HSA and ALEXA-488 was used in the labeling reaction.

Experimental setup

The experimental setup and the sample preparation procedure were described in detail by Kubitscheck et al. (2000). In short, specimens were observed using an inverted wide-field epi-fluorescence microscope (AXIOVERT 100 TV; Zeiss, Jena, Germany). The 488-nm line from an Ar^+-laser (model 2025, Spectra Physics, Darmstadt, Germany) was guided through an acousto-optical modulator (AOM, Model 304, Coherent, Santa Clara, CA) and a λ/4-plate, and over-illuminated the field iris diaphragm. For imaging, a planapochromatic objective lens (63×, NA 1.4, Zeiss) was used. The image of the iris diaphragm in the focal plane had a diameter of ~15 μm, over which the illumination intensity varied by ~10%, falling off rapidly at the border. The irradiance in the sample plane was adjusted to ~4–5 kW/cm^2. Fluorescence light was separated from the excitation light by a dichromatic beam splitter, and was detected after passing through an emission filter (505DRLP and 535RDF45, respectively; Omega Optical, Brattleboro, VT) by a cooled slow-scan CCD camera (QUANTIX, Photometrics, München, Germany, with a Kodak KAF 1400 grade 1 CCD chip, Rochester, NY). The light detection efficiency amounted to ~3% (Kubitscheck et al., 2000). The CCD wells translated 2.5 photoelectrons into one count.

Image acquisition was performed using an Apple Macintosh G3 computer using the IPLab software (Scanalytics Inc., Fairfax, VA). Image integration time was 5–20 ms. The illumination light beam was switched on only during image acquisition by means of the computer-controlled AOM (rise time 100 ns). Images were acquired either in the normal slow-scan mode with a frame repetition rate of ~4 Hz or in the high-speed framing (HSF) mode. For this, the major part of the CCD chip was masked immediately in front of the CCD coverglass such that only a small portion of the total chip area was exposed to light. After image acquisition the illuminated lines on the chip were shifted into the masked region that served as fast intermediate image storage. This process could be performed rapidly with a minimal shift time of 8 ms and was repeated eight times, resulting in a sequence of nine images acquired at a maximal repetition rate of ~80 Hz.

Characterization of protein labeling

The average number of fluorophores per HSA and P4K molecule, respectively, was determined by absorption spectroscopy. Molar absorption coefficients used amounted to $\epsilon_{280\ nm}$(HSA) = 33,100 $cm^{-1}\ M^{-1}$, ϵ_{495nm}(ALEXA-488) = 72,000 $cm^{-1}\ M^{-1}$, $\epsilon_{280\ nm}$(ALEXA-488) = 11,300 $cm^{-1}\ M^{-1}$, and $\epsilon_{280\ nm}$(P4K) = 258,700 $cm^{-1}\ M^{-1}$. The number of fluorophores per protein was also determined on a single molecule basis. To this end solutions of the various proteins with nanomolar concentrations were prepared in transport buffer, and aliquots of these solutions were placed on clean coverglasses. A small fraction of the proteins rapidly attached irreversibly to the glass surfaces, and the coverglasses were washed immediately. A small amount of transport buffer was added, and the coverglass was mounted on the microscope. Due to the low protein concentration applied, punctuate patterns of ALEXA-488 fluorescence were observed on the coverglass surfaces.

Nuclear import

3T3 cells were cultured in Dulbecco's minimum essential medium (Boehringer) at 37°C, 5% CO_2 and passaged every three days. For transport measurements, cells were used 24–48 h after seeding on coverglasses. Cells were permeabilized with digitonin according to Adam et al. (1990). Digitonin (Calbiochem, Bad Soden, Germany) was diluted in transport buffer to yield a final concentration of 50 μg/ml. For cell permeabilization, a coverslip with adhering cells was washed three times with ice cold transport buffer. Then the coverslip was incubated with 1 ml of the digitonin solution for 5 min on ice. After washing, coverslips were mounted upside down on glass slides, using spacers to create a little chamber containing 5 μl transport solution.

The transport solution, i.e., the medium in which cells were immersed for transport measurements, contained the transport substrate (P4K-ALEXA), oocyte lysate, an ATP-regenerating system and, in control experiments, 70 kDa TR-dextran (200 μg/ml). *Xenopus laevis* oocyte lysate was prepared as described by Newmeyer and Wilson (1991). The ATP-regenerating system comprised creatine phosphokinase (80 U/ml), creatine phosphate (10 mM), and ATP (2 mM). Solutions of creatine phosphate and ATP were freshly prepared in transport buffer before each experiment. A solution of creatine phosphokinase in transport buffer was stored in small aliquots at −20°C. The nucleus integrity was verified by exclusion of TR-dextran.

Nucleo-cytoplasmic transport was measured by confocal laser scanning microscopy (Leica TCS E; Leica Lasertechnik, Heidelberg, Germany) using dual channel detection, and a final concentration of P4K-ALEXA 488 of 100 μg/ml. A sample was prepared as described above, and was placed on the stage of the inverted microscope. By using a 100× oil-immersion objective lens (NA 1.3) the thickness of the confocal optical section was determined to be <1 μm. The 488-nm line of an argon-krypton laser was used for excitation of the ALEXA-488, emission was measured in the wavelength range of 510 to 530 nm. The 568-nm line of the argon-krypton laser excited red-fluorescence of TR-dextran, which was monitored above 590 nm. Images were recorded in the green channel at different time points after sample preparation.

For observation and tracking of single P4K molecules inside cell nuclei the sample was prepared as described above; however, P4K-ALEXA-488 was diluted in the oocyte lysate to a final concentration of ~1–10 nM, and TR-dextran was omitted to reduce the overall fluorescence background.

Localization procedures

The image of a point object like a single molecule has a complex 2D intensity profile in the image plane referred to as point spread function (PSF). The PSF limits the spatial resolution achievable by a microscope and can be determined experimentally by imaging a fluorescent subresolution object. The SNR of an image is determined by the brightness of the utilized probes, and specific instrument parameters for the integration time, detector pixel size, read-out rate, and photoelectron conversion factor and laser irradiance. We define the SNR of single molecule signals in the following way:

$$\mathrm{SNR} = \frac{I_0}{\sqrt{\sigma_{\mathrm{bg}}^2 + \sigma_{\mathrm{I_0}}^2}}, \qquad (1)$$

where I_0 designates the signal intensity of the maximum of the PSF above background, σ_{bg}^2 the variance of the background intensity values, and σ_{I0}^2 the variance of the maximum signal intensity above background; σ_{bg}^2 must be determined experimentally as described in detail by Kubitscheck et al. (1999).

If an area detector is positioned in the image plane the observed PSF can well be approximated by a 2D Gaussian function. By fitting a 2D Gaussian function to an observed 2D intensity profile of a subresolution object the object center can be determined with a very high accuracy, often 10–20 times smaller than the FWHM of the PSF. In our study a user-written analysis program was used to determine the central position of each subresolution object by fitting a 2D Gaussian function to the observed fluorescence intensity profile using a nonlinear χ^2-minimization routine (Press et al., 1992). However, because image acquisition is a stochastic process due to the inherent Poisson noise of light emission, the object position (x_c, y_c) that is found by the fitting algorithm is only an estimator for the true object position.

We define as particle localization accuracy that distance from the found object center, in which the true object center is located with a probability of 0.68. The localization accuracy depends strongly on the actual SNR. In case the fitting procedure is realized by χ^2-minimization algorithm, an analytical approximation for the localization accuracy of subresolution objects can be derived (Bobroff, 1986). Thereby an expectation value for the localization accuracy can be calculated as a function of the SNR. As we have shown recently, this expectation value presents an upper limit for the experimentally found localization accuracy (Kubitscheck et al., 2000). We have performed a respective analysis for our experimental setup and found that an SNR between 10 and 2 corresponds to a localization accuracy between 10 and 60 nm.

Monte Carlo simulation

A Monte Carlo simulation program for diffusion was based on the random number generator of L'Ecuyer with Bays-Durham shuffle that returns a uniform random deviate between 0 and 1, and the Box-Muller method was used for generating random deviates with a Gaussian distribution according to Press et al. (1992). The impermeable borders of the diffusion space were defined by an ellipsoid with main axes of 15, 20, and 6 μm length along *x*-, *y*-, and *z*-directions, respectively, corresponding to the size of a cell nucleus. Particle trajectories comprising 10^4 steps each were simulated assuming a diffusion constant of 2.5 $\mu m^2/s$ at time steps of 18 ms.

Mobility measurements by scanning microphotolysis

The immobile fraction of imported P4K molecules was measured by scanning microphotolysis (SCAMP) with a confocal laser scanning microscope as described by Wedekind et al. (1994). SCAMP is a combination of confocal laser scanning microscopy and fluorescence microphotolysis. A CLSM was equipped with an optical switch represented by an acousto-optical tunable filter, which was able to modulate the power of the laser beam in less than a microsecond, while the laser beam modulation and the scanning process were coordinated by a dedicated computer program. Thereby it was possible to vary the power of the laser beam by a factor >2000 during scanning at the precision of one resolution element. Here, large rectangular regions were slowly bleached into 3T3 cell nuclei, which had previously accumulated P4K-ALEXA. The time scale of bleaching was chosen so that the pool of mobile molecules in the bleached and unbleached nuclear region was completely depleted. The fraction of immobile P4K molecules was calculated by the ratio of the remaining fluorescence in unbleached nuclear regions and the prebleach intensity.

RESULTS

Prerequisites for single-molecule studies of intranuclear transport

Identification of single protein molecules by laser fluorescence microscopy

By using the fluorescence microscopic setup described in Materials and Methods single molecules of HSA, IgG, and the recombinant karyophilic protein P4K were identified by fluorescence measurements. All proteins were labeled with the same fluorophore, ALEXA-488. However, the labeling ratios varied in wide limits. Thus, HSA carried a mean number of 0.3 fluorophores per molecule, while the labeling ratio was 6.8 for IgG and 4.6 for P4K. Assuming that labeling is a random, non-cooperative process, a low labeling ratio such as 0.3 guarantees that virtually all of the labeled protein molecules carry only a single fluorophore, while the fractions of protein molecules carrying two or more fluorophores can be neglected.

ALEXA-labeled proteins were attached to coverslips and imaged by HSF at an integration time of 10 ms per frame. An example pertaining to HSA-ALEXA-488 is shown in Fig. 1. In the image stack three different fluorescence spots are seen which are presumably single HSA molecules attached to the glass surface (Fig. 1 *A*). In Fig. 1 *B* the integral fluorescence of the three observed spots is plotted versus the frame number. This reveals that the fluorescence of the spots bleached in a "digital" manner, as expected for individual fluorophore molecules, and thus provides strong evidence for the assumption that the spots represent single HSA molecules.

Analogous experiments were also performed with P4K and IgG. For each protein the fluorescence of individual spots was quantified in terms of counts above background. Furthermore, the total number of counts before photobleaching was determined. Using the overall detection efficiency and the photoelectron-to-digital unit conversion

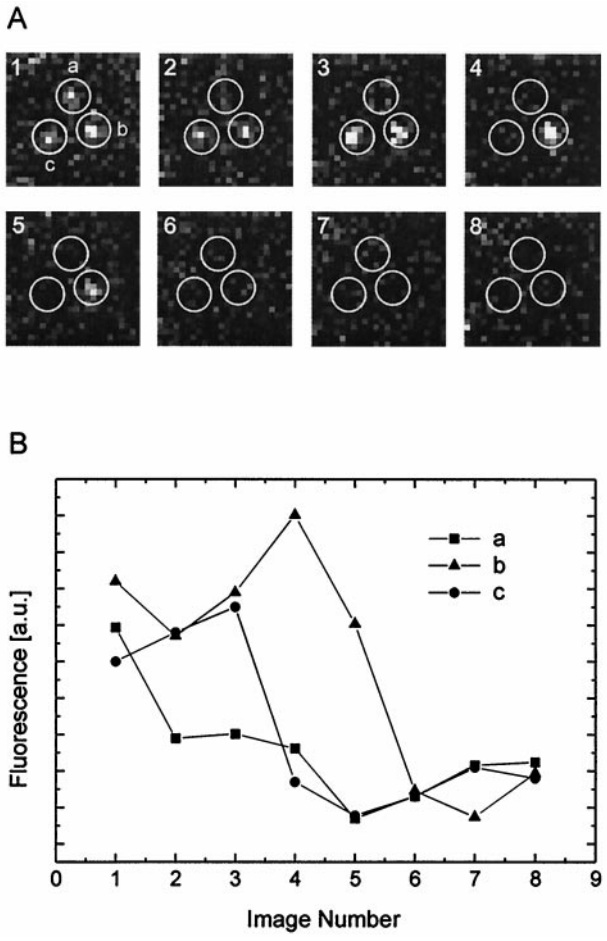

FIGURE 1 Fluorescence signals from HSA-ALEXA molecules. (*A*) Image series showing HSA-ALEXA molecules attached to a coverglass surface. Integration time for each frame was 10 ms. Three different fluorescence spots are marked. (*B*) Integral fluorescence signal above background for the three observed spots as a function of the frame number. The signals bleach in a single step.

factor of the CCD camera, the number of counts was converted into the absolute number of photons. The results of these experiments are displayed in Fig. 2 and summarized in Table 1. The number of photons emitted in 10 ms by the IgG molecules was found to be 5.7 ± 1.4 (mean ± SEM) times higher than the number of photons emitted by the HSA (Fig. 2, *A* and *C*). The time-integrated fluorescence signal of the IgG was 7.4 ± 0.3 times as high as the HSA signal (Fig. 2, *D* and *F*). The average of these two values is 6.5 ± 1.7, very similar to the labeling ratio of IgG (6.8 fluorophores per IgG molecule). The fluorescent spots pertaining to P4K-ALEXA molecules emitted, during an integration time of 10 ms, 4.3 ± 1.1 ($n = 350$) times more photons than those of HSA-ALEXA. The total number of photons emitted before photobleaching (Fig. 2, *B* and *E*) was 4.8 ± 0.3 times that of HSA-ALEXA. This indicated that P4K-ALEXA was labeled on the average with 4.6 ± 1.4 fluorophores, an assumption strengthened by spectrophotometric measurements yielding a mean labeling ratio of 3.9 ± 1.

Autofluorescence of intact and permeabilized cells

The detection and tracking of single fluorescently labeled molecules is essentially limited by the SNR (Kubitscheck et al., 2000). Because the number of photons emitted by an individual fluorophore before photobleaching is limited, the background fluorescence and its noise assume a decisive role and can easily prevent single-molecule detection. It was therefore important to determine the background fluorescence in the cells used in this study.

Three types of images were acquired at standard conditions (i.e., an object field of 5 × 5 μm, an irradiance of 5 kW/cm^2, and an integration time of 10 ms): "dark current images" (camera shutter closed), images of the specimen chamber containing only buffer, and images of intact and digitonin-permeabilized cells. From these the mean fluorescence and its standard deviation (SD) were derived. We found that cytoplasm and nucleus differed widely in their autofluorescence, even in digitonin-permeabilized cells. This can be directly recognized in images as displayed in Fig. 3 *A*. The values for the mean fluorescence and the SD are given in Fig. 3, *B* and *C*. The SD of dark images amounted to 6.1 counts, which is almost identical to the read-out noise of the camera. In intact and permeabilized cells the mean nuclear fluorescence was ~5- or 10-fold larger than that of the buffer. However, the respective SDs increased only by ~25%. In case of the cytoplasm both the mean fluorescence and its SD were 3–4 times larger than those of the nuclei. We conclude that the autofluorescence of nuclei was small enough not to compromise single molecule detection and tracking. In contrast, the autofluorescence of the cytoplasm was substantial and might interfere with single molecule measurements.

Identification and tracking of single protein molecules in the cell nucleus

Visualization of single protein molecules in the nucleus

The recombinant protein P4K contains a nuclear localization sequence and therefore is imported into nuclei of digitonin-permeabilized cells via the NPCs when the soluble transport factors are supplied in a cytosolic extract and metabolic energy is provided by addition of an ATP regenerating system (ARS). We incubated digitonin-permeabilized 3T3 cells with exceedingly small concentrations of P4K (1–10 nM) in the presence of cytosolic extract and ARS to achieve very small intranuclear P4K concentrations. Furthermore, imaging was started very briefly after addition of P4K to follow the appearance of P4K molecules in the nucleus from the very beginning. A representative example for the imaging of intranuclear P4K molecules is shown in

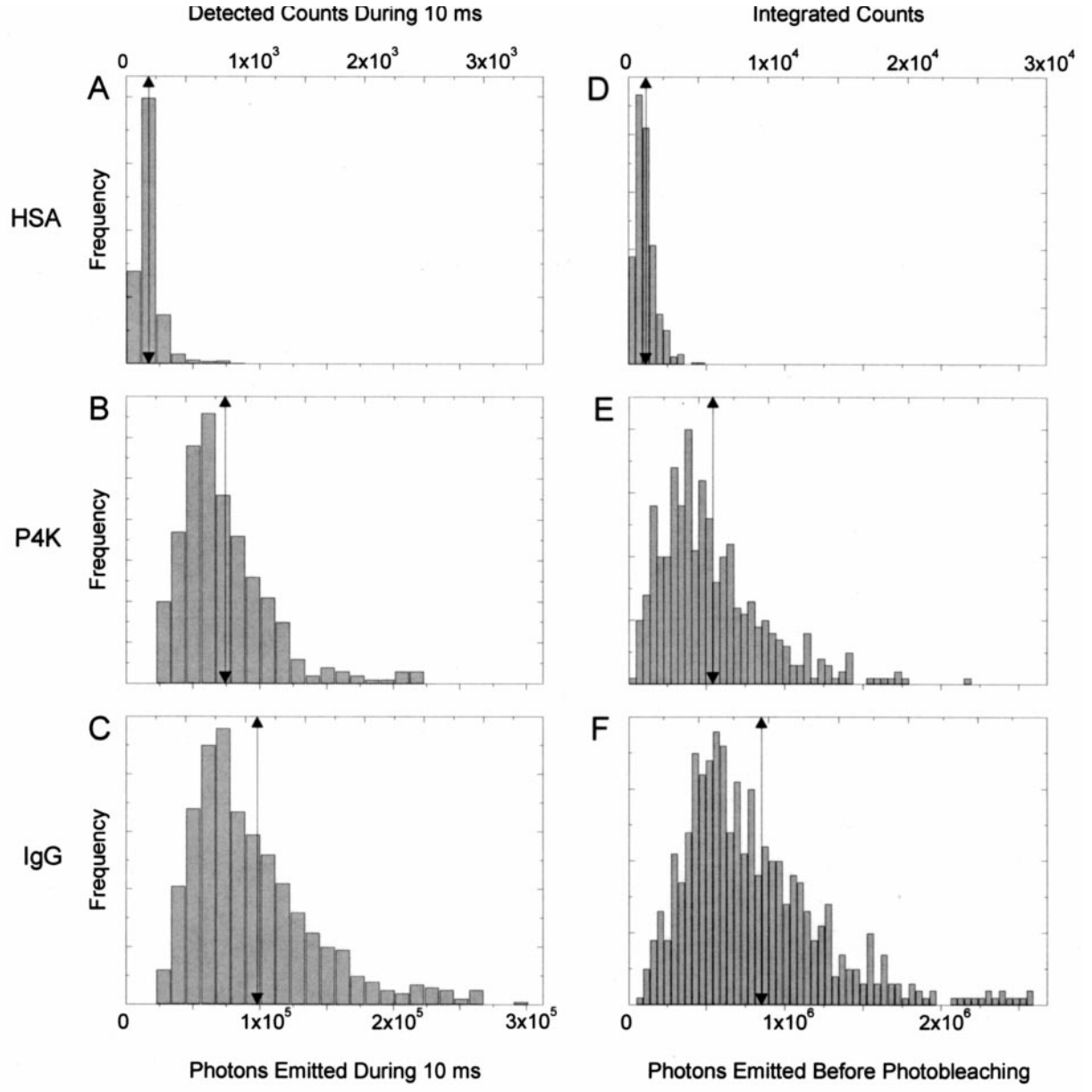

FIGURE 2 Frequency distributions of the single molecule signals for the examined proteins. Graphs *A–C* display the number of detected fluorescence counts, and of emitted photons, for the integration time interval of 10 ms for HSA-ALEXA (n = 643), P4K-ALEXA (n = 350), and IgG-ALEXA (n = 685), respectively. The data were obtained from image series such as shown in Fig. 1. The number of emitted photons was determined assuming a detection efficiency of 2.8%. Graphs *D–F* show the total number of emitted photons and the time-integrated number of detected fluorescence counts, before final photobleaching for HSA-ALEXA, P4K-ALEXA, and IgG-ALEXA, respectively. Mean values are indicated by arrows, and compiled in Table 1.

Fig. 4. The nucleus and its boundary can be recognized in the bright field image at the top of Fig. 4 *A*. The series of fluorescence images displayed below the bright field image was obtained at an integration time of 10 ms per image and a delay time of 8 ms between two subsequent images covering a total time of ~150 ms. The images show many clearly discernible spots that we identify on the basis of their intensity (see below) as diffraction-limited images of single P4K-ALEXA molecules. Three of the presumed P4K molecules were marked by arrows. An area is outlined and a surface plot of that area is given in Fig. 4 *B*. A close look at the image series reveals a whole range of mobility types. Some molecules are apparently mobile, entering the focal plane at some instance and moving around from frame to frame. Other molecules appear to be perfectly immobile during the observation time; they could be observed in more than 15 frames. Still other molecules appeared confined, although moving, to a small object region.

The fluorescence of individual immobile spots was quantified and found to amount on average to ~50% of that

TABLE 1 Results of single protein fluorescence measurements

Probe Molecule	Number of Photons/10 ms	Total Number of Photons
HSA-ALEXA 488	1.3×10^4	1.1×10^5
P4K-ALEXA 488	5.5×10^4	5.3×10^5
IgG-ALEXA 488	8.0×10^4	8.1×10^5

Molecules were attached to a cover glass surface and illuminated with an average laser power of 5 kW cm^{-2}. Given is the number of photons assuming an overall detection efficiency of 2.8% (Kubitscheck et al., 2000).

found for single P4K molecules immobilized at the water-glass interface (Fig. 2 *B*). A reduction of the fluorescence signal inside the nucleus was to be expected because of the refractive index mismatch (Hell et al., 1993), and also because the nucleus is a heterogeneous structure in which the fluorescence light of P4K molecules may be strongly scattered.

A substantial fraction of the P4K molecules appeared to be immobile. This is consistent with our previous photobleaching measurements (Rihs and Peters; 1989) yielding an immobile fraction of 32 ± 10% for P4K in HTC cells. We repeated such photobleaching measurements with the 3T3 cells used in this study and found a somewhat large yet still comparable immobile fraction of 45 ± 10% (data not shown).

Tracking of single protein molecules in the cell nucleus

Image stacks such as the one displayed in Fig. 4 were used to determine the trajectories of single P4K molecules. Each spot, which did not derive from a larger aggregate but, judged by its brightness, was due to a single P4K molecule and which could be followed over several images of the stack, was localized at nanometer precision by the procedure described in Materials and Methods. The average SNR of P4K molecule signals, SNR_{P4K}, from a depth of ~5–10 μm inside the nucleus was determined according to Eq. 1 to be between 2 and 10, yielding a localization accuracy of 10–60 nm with a mean value of $\sigma_{acc} = 35$ nm (Kubitscheck et al., 2000). Each trajectory was characterized by a set of coordinates $\{x_i, y_i\}$, where $1 \leq i \leq N$, with N denoting the number of observations of an individual molecule. For each trajectory, a set of square displacements, $r^2(t_{lag})$, between two positions separated by the time lag t_{lag} was obtained. The time lag was given by $t_{lag} = n(t_{ill} + t_{delay})$, where t_{ill} denotes the integration and t_{delay} the delay time between two successive subframe acquisitions. To reduce the noise the square displacements within a single trajectory were averaged for identical lag times resulting in the mean-square displacements, $MSD(t_{lag})$ for that trajectory. This procedure implies that the short-range $MSD(t_{lag})$ is more accurately determined than the long-range $MSD(t_{lag})$.

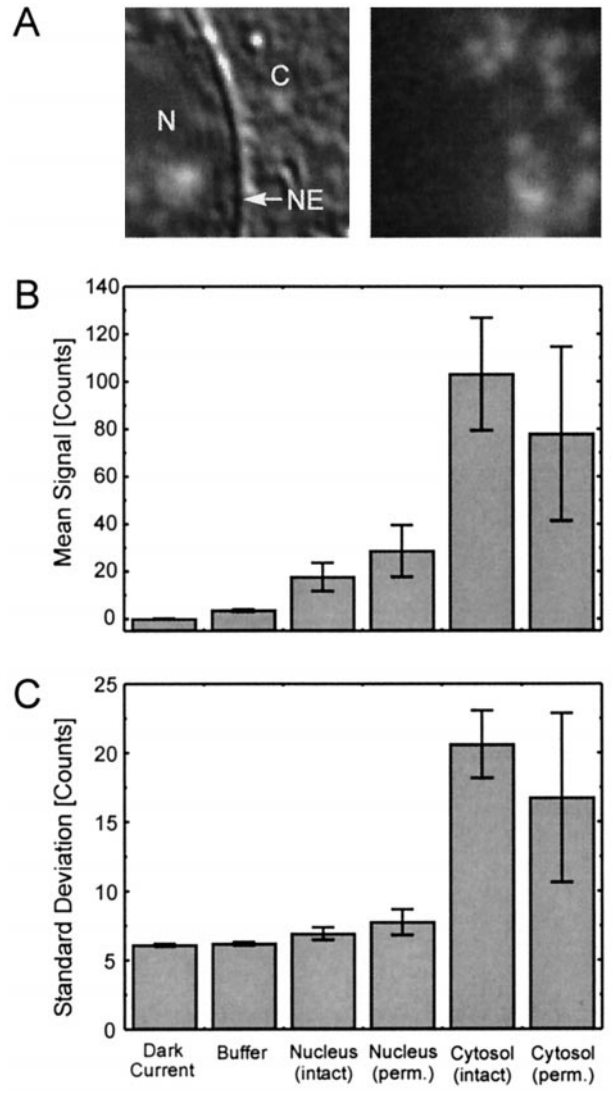

FIGURE 3 Cellular autofluorescence. (*A*) Bright field (*left*) and autofluorescence (*right*) image of a permeabilized cell (N, nucleus; NE, nuclear envelope; C, cytoplasm). (*B*) Mean signals and (*C*) averaged standard deviations from 20 single measurements. Images were acquired using a typical irradiance of 5 kW cm^{-2} and an image integration time of 10 ms. The main contribution to image noise for dark images, buffer images, and images from cell nuclei is the CCD camera readout noise. This situation is different for the inhomogeneous and high cytoplasmic autofluorescence.

In the case of free Brownian motion in two dimensions the diffusion coefficient D is related to the MSD by

$$MSD(t_{lag}) = 4Dt_{lag} \quad (2)$$

A linear relationship between MSD and time therefore indicates free Brownian motion, and can be used to derive the diffusion coefficients from single molecule trajectories. However, if molecular transport is not based on free diffusion but, for instance, on confined diffusion or directed flow, the analytical form of $MSD(t_{lag})$ versus time is differ-

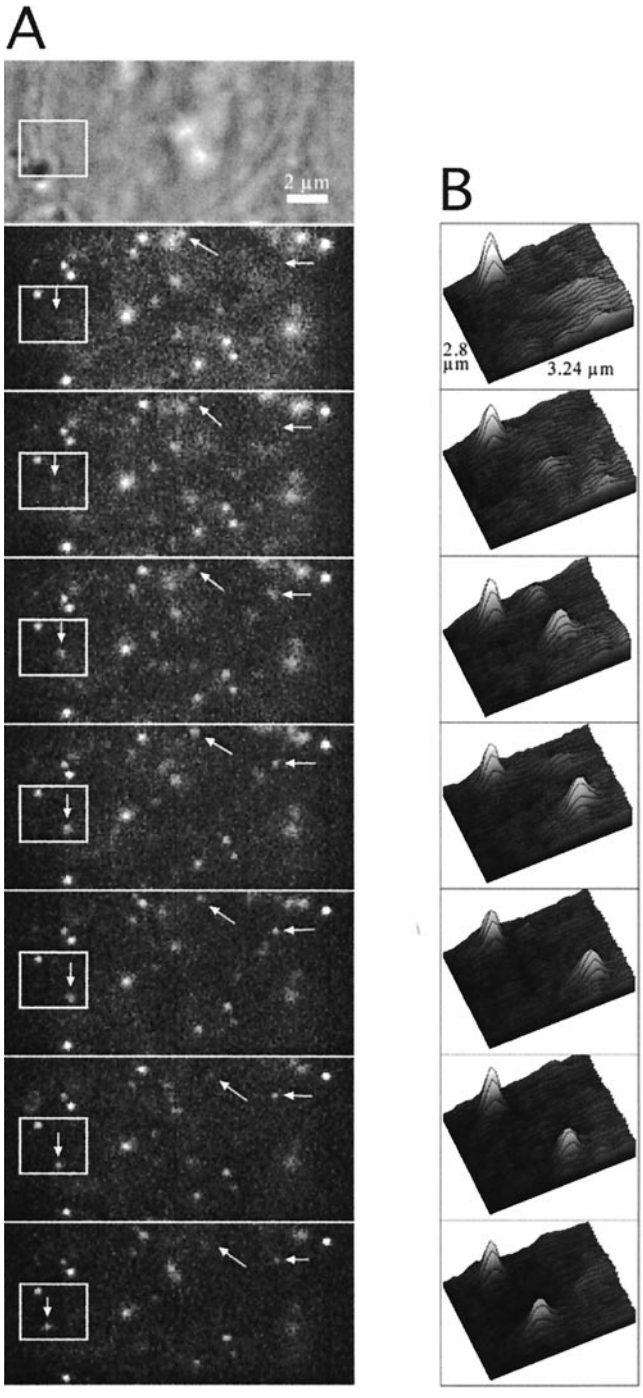

FIGURE 4 Single P4K molecules inside a cell nucleus detected by HSF imaging series by epifluorescence. (*A*) The topmost image was taken in bright field mode to identify the nuclear envelope. Below, a typical HSF image series acquired 5 min after starting the import process is shown. The image series was taken with an integration time of 10 ms per image and a delay time of 8 ms between two subsequent images. Therefore, the fluorescence image series covers a time window of ~120 ms; the total object field size is 17.3 × 8.1 μm^2. The image shows many clearly discernible diffraction-limited spots that we interpret as images of single P4K-ALEXA molecules. The arrows mark three different moving molecules. (*B*) Surface plot representation of the outlined (and 3 × 3 Gauss kernel smoothed) image region in (*A*).

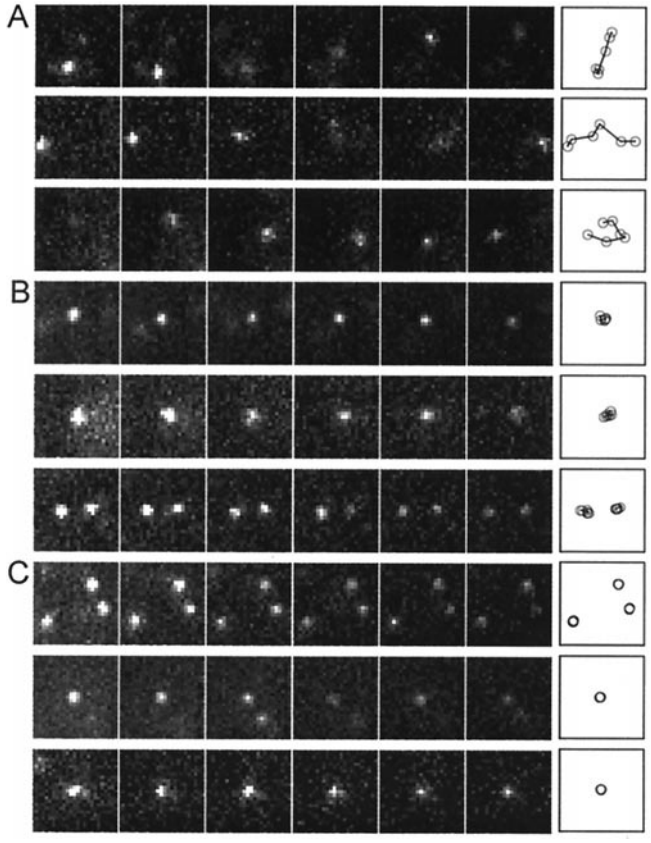

FIGURE 5 Representative examples of molecular motions in cell nuclei obtained by HSF imaging. (*A*) Apparently freely diffusing P4K molecules. Image integration time was 10 ms, and lag time between two successive images was 8 ms. The shown object field size is 2.7 × 2.7 μm^2. (*B*) Examples for molecules, whose movement was presumably restricted. (*C*) Images of molecules that appeared immobile on the time scale of observation. The right-hand image shows the molecular trajectory.

ent (Saxton and Jacobson, 1997). Indeed, an inspection of various trajectories of P4K in the nucleus suggested that different mobility classes exist. This is illustrated in Fig. 5, giving examples of relatively fast-moving, possibly freely diffusing molecules (Fig. 5 *A*); of molecules swaying in a confined region (Fig. 5 *B*); and of molecules that were immobile on the time scale of the observation (Fig. 5 *C*). It may be noted, however, that the classification of molecular mobility classes is somewhat arbitrary. Even freely diffusing molecules show all kinds of random trajectories resembling by chance those of free, restricted, or immobile molecules (Saxton and Jacobson, 1997).

Analysis of molecular trajectories in terms of diffusion coefficients

Validation of the experimental and theoretical methods by computer simulation and measurements on model systems

In the experimental setup used in this study only those P4K molecules that happened to move into or across the focal

plane could be observed and tracked. More precisely, the present setup imaged a slice having its center in the focal plane and extending ~0.8 μm in the direction of the optical axis. The P4K molecules, however, could distribute over a much larger space, namely the complete nuclear volume. This raised the possibility that our method might be biased for detecting slowly moving particles, which remained in the imaged slice during the observation time. In order to test for this possibility the experimental situation was simulated by numerical methods. The simulation considered point objects undergoing free diffusion in a volume corresponding to that of a nucleus, while observation was restricted to a slice corresponding in its dimensions to the experimentally realized optical section.

In the computer simulations the nucleus was approximated by an ellipsoid having main axes of 7.5, 10, and 3 μm (x, y, z) length. Particle trajectories within this volume were simulated by standard Monte Carlo methods (Saxton, 1997, cf. Materials and Methods) assuming a diffusion constant of $D = 2.5\ \mu m^2/s$. The "observation slice" was assumed to have a thickness of 0.8 μm, as indicated in Fig. 6 *A*. Whenever a particle happened to be within the observation slice its trajectory was recorded. Fig. 6 *B* shows the averaged mean-square displacements of the first five time steps of five trajectories with 10^4 steps each; the solid line is a fit to the data according to Eq. 2. The fit yielded a diffusion constant of $D = 2.49 \pm 0.02\ \mu m^2/s$, very closely approaching the "true" one, and thus supporting the validity of our experimental approach.

We extended the analysis of molecular trajectories by using a more sophisticated approach. Although there are various procedures for evaluating MSD or jump distance data in terms of diffusion coefficients (for review, see Saxton and Jacobson, 1997), we chose the method of Cherry and co-workers (Anderson et al., 1992; Wilson et al., 1996; Smith et al., 1999). It is based on analyzing the probability distribution of the absolute molecular displacements as a function of t_{lag}. The probability distribution indicates whether fractions of molecules with different modes of motion are present. This approach allows conclusions from relatively short trajectories, because the data from all observed trajectories are gathered. $p(r, t)dr$ is defined as the probability, that a particle starting at the origin will be found at time t within a shell of radius r and a width dr. For random diffusion in two dimensions

$$p(r, t)dr = \frac{1}{4\pi Dt} e^{-r^2/4Dt} 2\pi r dr \qquad (3)$$

The frequency distribution $p(r, t)dr$ is constructed by counting the number of displacements within the interval $[r, r + dr]$ for each value of t_{lag} from all observed trajectories. This was performed for the sections of the point object trajectories that were detected in the observation slice. Fig. 6, *C–F* shows the frequency distributions of jump distances that were determined on the basis of five trajectories with 10^4 single steps at lag times of 18, 54, 90, and 126 ms corresponding to those the experimental image stacks. The solid line is the result of a fit according to Eq. 3 assuming a single mobile fraction of molecules. The thus-determined diffusion constants of 2.49 ± 0.03, 2.46 ± 0.08, 2.41 ± 0.07, and 2.29 ± 0.09 $\mu m^2/s$ are based on 4162, 2100, 1057, and 547 evaluated jump distances, respectively. The number of positions that is found in the detection slice is decreasing with increasing lag time, due to the fact that the probability of finding a mobile particle in the detection slice is decreasing with time. Thus, the more sophisticated analysis suggested that the experimental method used in this study is valid, and only very slightly biased for selecting molecules with small diffusion coefficients.

Experimentally, the methods used were tested by measurements of model systems. These consisted of well-defined particles or molecules dissolved in media of known viscosity. In particular, fluorescent microbeads (14-nm diameter) were dispersed in 50% glycerol/buffer mixtures and GFP molecules were dissolved in 80% glycerol/buffer mixtures. The viscous solutions were placed as a thick layer between a glass slide and a coverslip, and trajectories of single particles or molecules were recorded by HSF. Single fluorescent spots were localized and analyzed as described above. Some of the experimental data have been published previously (Kubitscheck et al., 2000). Here, the data were reevaluated by deriving the jump distance frequency distributions of microbeads and molecules within lag times 11, 33, 44, and 66 ms and fitting them by Eq. 3 (data not shown). We could fit the frequency distributions assuming a single diffusion constant. The total number of measured jump distances decreased with increasing lag time, because the mobile particles escape with time from the detected optical slice. The diffusion coefficients determined both for the microbeads (*filled circles* in Fig. 8) and GFP molecules (*crosses* in Fig. 8) were independent of the lag time.

Analysis of intranuclear protein trajectories

Having validated the experimental and theoretical methods we applied them to the intranuclear transport of P4K. For the acquisition of molecular trajectories in the nucleus the described HSF method was used yielding short lag times of ≥18 ms. In addition, the normal imaging mode of the CCD camera was used to extend t_{lag} up to 1500 ms.

On the basis of HSF stacks, the jump distance frequency distribution analysis was applied to 230 trajectories of individual P4K molecules. Four of the seven resulting histograms are presented in Fig. 7, *A–D*, covering lag times between 18 and 126 ms. In contrast to the simulated data (Fig. 6) and the experimental data of microbeads and GFP, the data for the intranuclear motion of P4K molecules could not adequately be fitted by Eq. 3, when only a single mobile

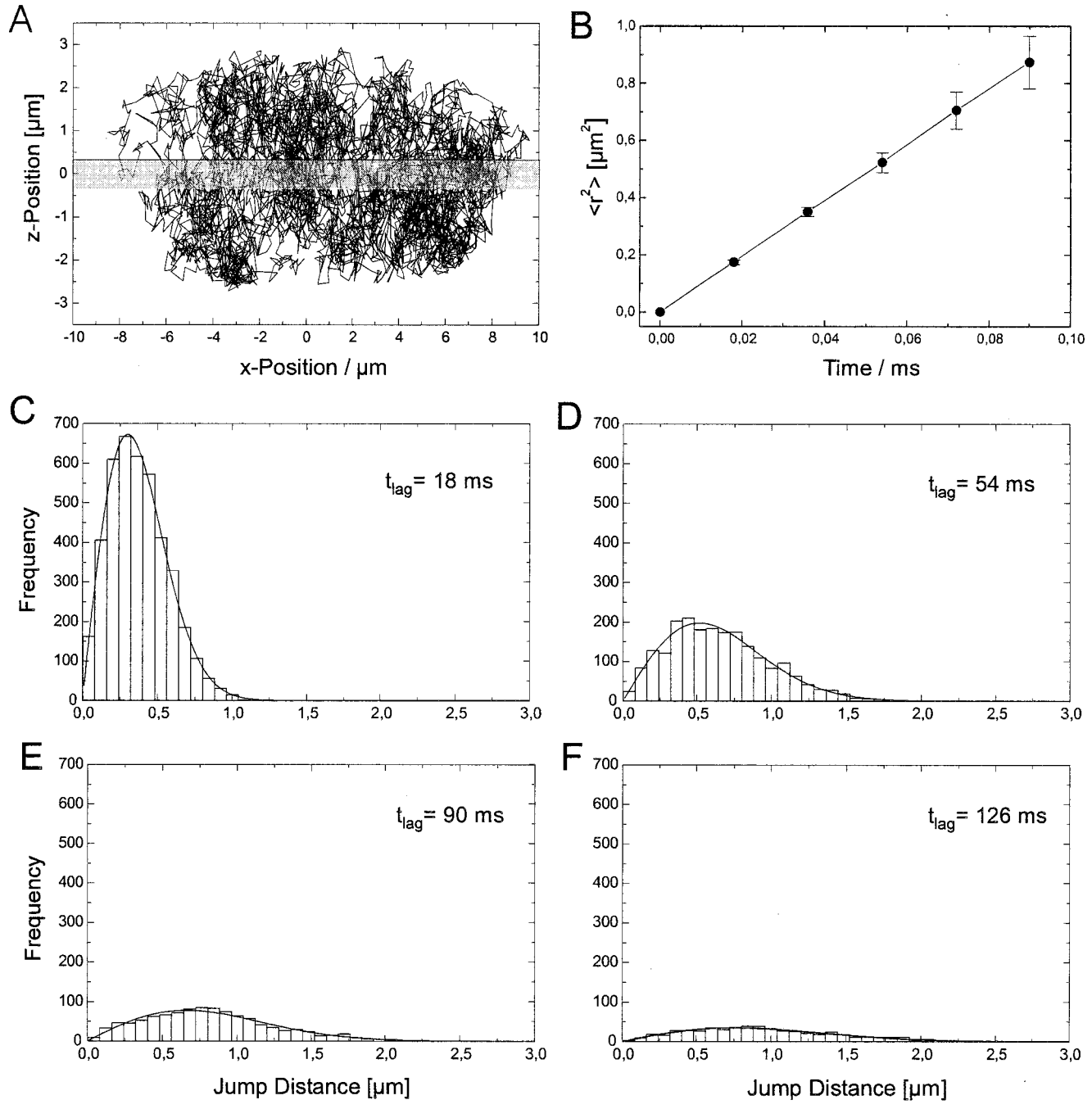

FIGURE 6 Computer simulation of diffusion within the cell nucleus. A cell nucleus was represented by an ellipsoid with main axes of 7.5, 10, and 3 μm along *x*-, *y*-, and *z*-directions, respectively. (*A*) Projection of a single trajectory with 10^4 steps onto the *xz*-plane. Particles were assumed to move with a diffusion constant of $D = 2.5$ $\mu m^2/s$ within the nucleus. For analysis only particle positions within an "observation slice" of 0.8 μm thickness (see shadowed region) were considered. (*B*) Averaged mean-square displacements of the first five time steps of five trajectories; the solid line shows the result of a fit according to Eq. 2 ($D = 2.49 \pm 0.02$ $\mu m^2/s$). *xy*-positions from steps within the observation slice were used for analysis in jump distance frequency histograms. (*C–F*) Frequency distributions of jump distances $p(r, t_{lag})dr$ that were determined on the basis of five trajectories with 10,000 single steps with lag times of 18, 54, 90, and 126 ms, respectively. Solid lines indicate the result of a fit according to Eq. 3 assuming a single mobile fraction of particles.

fraction was assumed. Rather, it was necessary to assume at least three populations (1–3) with widely differing diffusion coefficients D_1, D_2, and D_3. One fraction of molecules appeared to be immobile within the localization accuracy σ_{acc}, i.e., $D_1 \approx 0$. More precisely, due to the finite localization accuracy of $\sigma_{acc} = 35$ nm, even completely immobile particles virtually move within a small region. The jump distance probability distribution of immobile mole-

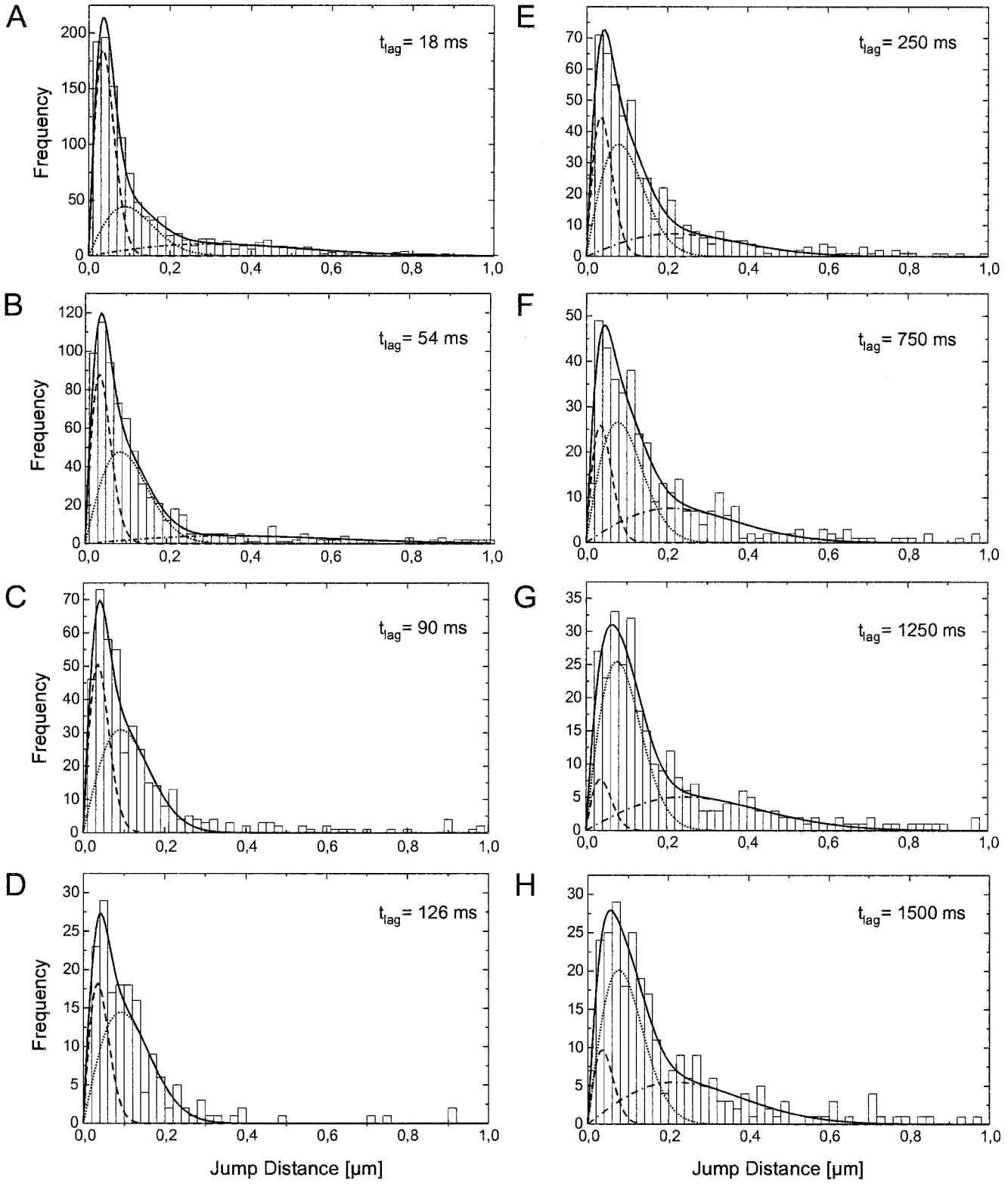

FIGURE 7 Jump distance frequency distributions for the P4K molecules in permeabilized cell nuclei as function of lag time, t_{lag}. Three modes of molecular motions were required for a satisfactory fit of the displacements after 18 ms (*A*), 36 ms (not shown), and 54 ms (*B*). One fraction of molecules appeared to be immobile within our localization accuracy (*dashed line*). Additional consideration of a second fraction of molecules with a diffusion coefficient D_2 according to Eq. 3 was not sufficient to describe the data (*dotted line*). For a satisfactory fit we had to presuppose a third fraction with a higher mobility D_3 (*dot-dashed line*). Hence, the observed frequency distributions were finally fitted by the sum of the immobile and two mobile fractions (*solid line*). Furthermore, 5% of the jump distances were >1 μm at short lag times, and were due to even faster molecules. The frequency distributions

cules is described by the time-independent probability distribution:

$$p_{\mathrm{im}}(\mathbf{r})\mathrm{d}\mathbf{r} = \frac{N_{\mathrm{im}}}{\sigma_{\mathrm{acc}}^2} e^{-\mathrm{r}^2/(2\sigma_{\mathrm{acc}}^2)} r\mathrm{d}r \qquad (4)$$

A fraction of ~5% of the jump distances were >1 μm within 18 ms. Such rapid molecules were detected in two subsequent images maximally, and are characterized by diffusion coefficients of >10 $\mu m^2/s$. Due to the relatively infrequent occurrence, these could not be analyzed further.

Using the normal readout mode of the CCD camera, molecular trajectories were obtained for lag times between 250 ms and 1500 ms. In order to satisfactorily fit the data to Eq. 3 it was again necessary to assume one immobile population and two mobile populations (Fig. 7, *E* and *F*). The complete results of the analysis, i.e., the diffusion coefficients and fractions of populations 1–3, are compiled in Table 2.

A further major result of the analysis, already obvious from Table 2, is illustrated in Fig. 8: for intranuclear transport the diffusion coefficients depended on the lag time, in contrast to free diffusion. This indicates that diffusion in the nucleus is not "free," but restricted. Such restriction can be brought about by physical parameters such as barriers and/or chemical parameters such as association-dissociation reactions (for review, see Saxton and Jacobson, 1997). At such conditions the dependence of the diffusion coefficient on the lag time can be described by (Bouchaud and Georges, 1990; Feder et al., 1996):

$$D = \frac{\Gamma}{4} t^{\alpha-1} \qquad (5)$$

Here Γ designates the transport coefficient, and α the factor quantifying the time dependence of the diffusion coefficient. In the underlying model diffusion is free at short times but slowed down at longer times, when the effect of barriers or binding becomes more dominant. The physical assumption behind Eq. 5 is that the diffusion space comprises a random array of continuously changing binding sites with such a broad distribution of association energies that no average residence time per trap can be defined; α quantifies the degree of the mobility restriction. For $\alpha = 1$ the motion reflects unrestricted Brownian diffusion with a constant diffusion coefficient, $D = 1/4\Gamma$. A fit according to Eq. 5 to the time-dependent diffusion coefficients, $D_2(t_{\mathrm{lag}})$ and $D_3(t_{\mathrm{lag}})$, resulted in values of α close to zero for the two mobile fractions. The transport coefficients correspond to values of a diffusion coefficient of $D_2(t = 10\ \mathrm{ms}) = 0.45\ \mu m^2/s$ and $D_3(t = 10\ \mathrm{ms}) = 7\ \mu m^2/s$, respectively. In contrast to these results, fits according to Eq. 5 to the control data resulted in α values of $\alpha_{\mathrm{beads}} = 0.9 \pm 0.04$, $\alpha_{\mathrm{GFP}} = 1 \pm 0.1$, and $\alpha_{\mathrm{sim}} = 0.97 \pm 0.01$ for microbeads, GFP (data not shown for clarity of the graph), and simulation data, respectively.

TABLE 2 Mobility of single P4K molecules inside cell nuclei

	Population 1		Population 2		Population 3	
Time Lag (ms)	D_1 ($\mu m^2/s$)	f_1 (%)	D_2 ($\mu m^2/s$)	f_2 (%)	D_3 ($\mu m^2/s$)	f_3 (%)
18	0	48	0.220	29	2.460	23
36	0	40	0.107	39	2.052	21
54	0	36	0.069	48	1.167	17
72	0	41	0.069	59	—	—
90	0	38	0.047	62	—	—
108	0	33	0.033	67	—	—
126	0	32	0.034	68	—	—
144	0	22	0.029	78	—	—
250	0	26	0.012	48	0.093	26
750	0	20	0.004	45	0.030	35
1250	0	8	0.0023	56	0.024	36
1500	0	11	0.0019	50	0.016	40

Results of the analysis of the time-dependent frequency distributions of the jump distances as a function of time shown in Fig. 8. Fits were performed according to Eqs. 3 and 4 considering, respectively, one and two mobile fractions. Errors range from 10 to 30%.

DISCUSSION

Our work establishes a novel approach for obtaining insight into dynamic processes within the cell nucleus: single fluorescently labeled protein molecules were visualized and tracked after their signal-mediated import into nuclei of digitonin-permeabilized 3T3 cells. Frequently, autofluorescence may prevent the detection of single molecules in cellular systems. Fortunately, however, the autofluorescence of nuclei was found to be very small, not interfering with single molecule detection. The optimization of the experimental setup comprising an efficient fluorescence excitation, highly sensitive fluorescence detection, short image acquisition times, and high frame rates further promoted single molecule detection. The upper limit of diffusion coefficients that may presently be detected by our setup is determined by the frame repetition time and the mean-square distance that the molecules move during the image integration time. On this basis it is estimated to be 4 $\mu m^2/s$. Similarly, the lower limit is estimated to be $10^{-3}\ \mu m^2/s$.

for lag times 90 and 126 ms were fitted by assuming only the immobile and one mobile fraction (*C, D*). Long lag time experiments (*E–H*): from normal image sequences the trajectories of single P4K molecules were determined, and the corresponding jump distance frequency distributions shown in *E–H* for the lag times of 250, 750, 1250, and 1500 ms, respectively. Again, a satisfactory fit to the jump distance data required three fractions. Results of the jump distance analysis were compiled in Table 2.

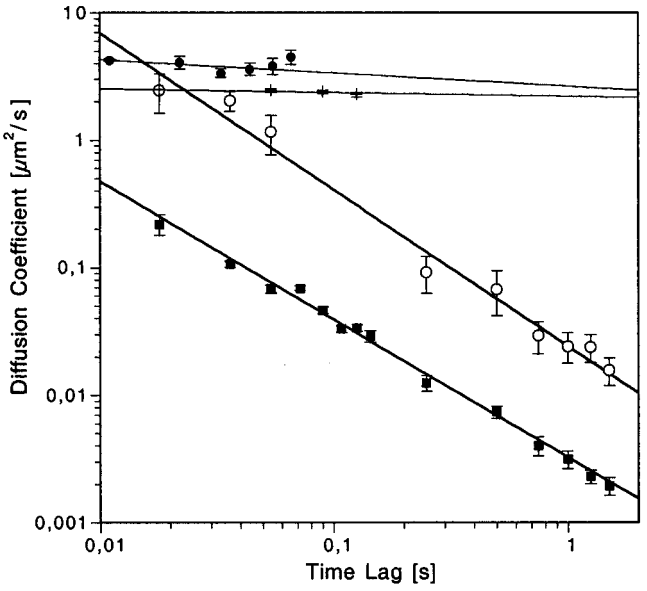

FIGURE 8 Double logarithmic plot of the determined diffusion constants versus lag time, t_{lag}. Diffusion coefficients were determined by the jump distance frequency distribution analysis as a function of lag times. The diffusion constants from the computer simulation (*crosses*, data from Fig. 6), and from microbead experiments (*filled circles*) were constant with lag time. Data from GFP experiments coincided with the symbols, and are not shown for clarity of the graph. The diffusion constants from the P4K molecules in cell nuclei ($D_2(t_{lag})$ and $D_3(t_{lag})$ indicated by *filled squares* and *open circles*, respectively) were decreasing with time (see Fig. 7 and Table 2). Solid lines represent fits to the data according to Eq. 5.

How molecules move around in the cell nucleus is still controversial (for review, see Daneholt, 1999; Pederson, 2000), and a wide range of mechanisms including free diffusion, restricted diffusion, and motor protein-mediated active transport has been discussed. Using the comparatively "inert" recombinant protein, P4K, we observed only diffusional motion. However, within this category a range of modes was detected. Thus one population of molecules appeared to be immobile within the range of our spatial resolution of ~35 nm, while at least three different mobile fractions were detected. Two of the mobile fractions, $f_{mob,1}$ and $f_{mob,\ 2}$, were analyzed quantitatively in terms of time-dependent diffusion coefficients. The corresponding movements appeared to be severely restricted. We assume that the constraints were due to association with intranuclear supramolecular structures with restricted mobility (Phair and Misteli, 2000). A good candidate for this is chromatin, which has been shown to undergo anomalous, restricted motion (Marshall et al., 1997). Fraction $f_{mob,2}$ was more mobile, with diffusion coefficients in the range of 1–2 $\mu m^2/s$ in the time range of 100 ms. This corresponds to a 20-fold slower movement than compared to diffusion in dilute buffer solutions. However, the diffusion coefficient of fraction $f_{mob,2}$ was also decreasing with time. The third mobile fraction, $f_{mob,3}$, of ~5% moves very fast with jump distances >1 μm within 18 ms. Such fast molecules were detected in two subsequent images maximally, and are characterized by diffusion coefficients of >10 $\mu m^2/s$. Fractions $f_{mob,2}$ and $f_{mob,3}$ presumably correspond to those mobile fractions, which were detected by previous measurements on intranuclear protein or tracer mobility (Schulz and Peters, 1987; Rihs and Peters, 1989; Seksek et al., 1997; Phair and Misteli, 2000). These measurements yielded diffusion coefficients 10- to 100-fold smaller than those measured in dilute buffer. Table 2 shows that the immobile fraction decreases with time from 48% to 10%, while the mobile fractions increase. This indicates that the probe molecules change their mode of motion, consistent with the assumption of successive association/dissociation events during the observation time.

The presented work demonstrates for the first time that it is feasible to observe the motion of single protein molecules within complex biological systems, such as cell nuclei. In contrast to methods such as photobleaching or fluorescence correlation spectroscopy, in our approach molecular displacements are detected well below the optical resolution limit, different types of motions can be differentiated, and very low tracer molecule concentrations may be used. We anticipate that further studies will provide a better understanding of both intranuclear transport mechanisms and submicroscopic topography.

Support from the Deutsche Forschungsgemeinschaft (DFG Grant Ku 975/3-1) and from the Volkswagen-Stiftung is gratefully acknowledged.

REFERENCES

Abney, J. R., B. Cutler, M. L. Fillbach, D. Axelrod, and B. A. Scalettar. 1997. Chromatin dynamics in interphase nuclei and its implications for nuclear structure. *J. Cell Biol.* 137:1459–1468.

Adam, S., R. Sterne-Marr, and L. Gerace. 1990. Nuclear protein import in permeabilized mammalian cells requires soluble cytoplasmic factors. *J. Cell Biol.* 111:807–816.

Anderson, C. M., G. N. Georgiou, I. E. G. Morrison, G. V. W. Stevenson, and R. J. Cherry. 1992. Tracking of cell surface receptors by fluorescence digital imaging microscopy using a charge-coupled device camera. Low-density lipoprotein and influenza virus receptor mobility at 4°C. *J. Cell Sci.* 101:415–425.

Axelrod, D., D. E. Koppel, J. Schlessinger, E. Elson, and W. W. Webb. 1976. Mobility measurement by analysis of fluorescence photobleaching recovery kinetics. *Biophys. J.* 16:1055–1069.

Berg, H. C. 1983. Random Walks in Biology. Princeton University Press, Princeton, New Jersey.

Buchenau, P., H. Saumweber, and D. J. Jovin. 1997. The dynamic nuclear redistribution of an hnRNP K-homologous protein during *Drosophila* embryo development and heat-shock. Flexibility of transcription sites in vivo. *J. Cell Biol.* 137:291–303.

Bobroff, N. 1986. Position measurement with a resolution and noise-limited instrument. *Rev. Sci. Instrum.* 57:1152–1157.

Bouchaud, J.-P., and A. Georges. 1990. Anomalous diffusion in disordered media: statistical mechanisms, models, and physical applications. *Phys. Rep.* 195:127–193.

Cherry, R. 1993. How to detect nonrandom motion of proteins in membranes. *Biophys. J.* 64:1651–1652.

Daneholt, B. 1999. Pre-mRNP particles: from gene to nuclear pore. *Curr. Biol.* 9:R412–R415.

Dietzel, S., A. Jauch, D. Kienle, G. Qu, H. Holtgreve-Grez, R. Eils, C. Munkel, M. Bittner, P. S. Meltzer, J. M. Trent, and T. Cremer. 1998. Separate and variably shaped chromosome arm domains are disclosed by chromosome arm painting in human cell nuclei. *Chromosome Res.* 6:25–33.

Edidin, M., Y. Zagyansky, and T. J. Lardner. 1976. Measurement of membrane protein lateral diffusion in single cells. *Science*. 191: 466–468.

Elson, E. L., and D. Magde. 1974. Fluorescence correlation spectroscopy. I. Conceptual basis and theory. *Biopolymers.* 13:1–27.

Feder, T. J., I. Brust-Mascher, J. P. Slattery, B. Baird, and W. W. Webb. 1996. Constrained diffusion or immobile fraction on cell surfaces: a new interpretation. *Biophys. J.* 70:2767–2773.

Hell, S., G. Reiner, C. Cremer, and E. H. K. Stelzer. 1993. Aberrations in confocal fluorescence microscopy induced by mismatches in refractive index. *J. Microsc.* 169:391–405.

Ishii, Y., and T. Yanagida. 2000. Single molecule detection in life science. *Single Mol.* 1:5–16.

Jacobson, K., Z. Derzko, E. S. Wu, Y. Hou, and G. Poste. 1976. Measurement of the lateral mobility of cell surface components in single, living cells by fluorescence recovery after photobleaching. *J. Supramol. Struct.* 5:565–576.

Jacobson, R. H., X-J. Zhang, R. F. DuBose, and B. W. Matthews. 1994. Three-dimensional structure of β-galactosidase from *E. coli*. *Nature.* 369:761–766.

Kubitscheck, U., O. Kückmann, T. Kues, and R. Peters. 2000. Imaging and tracking of single GFP molecules in solution. *Biophys. J.* 78:2170–2179.

Kubitscheck, U., T. Kues, and R. Peters. 1999. Visualization of the nuclear pore complex and its distribution by confocal laser scanning microscopy. *Methods Enzymol.* 307:207–230.

Kubitscheck, U., P. Wedekind, O. Zeidler, M. Grote, and R. Peters. 1996. Single nuclear pores visualized by confocal microscopy and image processing. *Biophys. J.* 70:2067–2077.

Lamond, A. I., and W. C. Earnshaw. 1998. Structure and function of the nucleus. Science 280:547–553.

Lang, I., M. Scholz, and R. Peters. 1986. Molecular mobility and nucleocytoplasmic flux of macromolecules in hepatoma cells. *J. Cell Biol.* 102:1183–1190.

Manuelidis, L. 1990. A view of interphase chromosomes. *Science.* 250: 1533–1540.

Marshall, W. F., A. Straight, J. F. Marko, J. Swedlow, A. Dernburg, A. Belmont, A. W. Murray, D. A. Agard, and J. W. Sedat. 1997. Interphase chromosomes undergo constrained diffusional motion in living cells. *Curr. Biol.* 7:930–939.

Mattaj, I. W., and L. Englmeier. 1998. Nucleocytoplasmic transport: the soluble phase. *Annu. Rev. Biochem.* 67:265–306.

Mehta, A. D., M. Rief, J. A. Spudich, D. A. Smith, and R. M. Simmons. 1999. Single-molecule biomechanics with optical methods. *Science.* 283:1689–1695.

Meseth, U., T. Wohland, R. Rigler, and H. Vogel. 1999. Resolution of fluorescence correlation measurements. *Biophys. J.* 76:1619–1631.

Newmeyer, D. D., and K. L. Wilson. 1991. Egg extracts for nuclear import and nuclear assembly reactions. *Meth. Cell Biol.* 36:607–635.

Nie, S., and R. N. Zare. 1997. Optical detection of single molecules. *Annu. Rev. Biophys. Biomol. Struct.* 26:567–596.

Pederson, T. 2000. Diffusional protein transport within the nucleus: a message in the medium. *Nat. Cell Biol.* 2:E73–E74.

Peters, R. 1986. Fluorescence microphotolysis to measure nucleocytoplasmic transport and intracellular mobility. *Biochim. Biophys. Acta.* 864: 305–359.

Peters, R., J. Peters, K. H. Tews, and W. Bähr. 1974. A microfluorimetric study of translational diffusion in erythrocyte membranes. *Biochim. Biophys. Acta.* 367:282–294.

Peters, R., and M. Scholz. 1991. Fluorescence photobleaching techniques. *In* New Techniques of Optical Microscopy and Microspectroscopy. R. J. Cherry, editor. Macmillan Press, London. 199–228.

Phair, R. D., and T. Misteli. 2000. High mobility of proteins in the mammalian cell nucleus. *Nature.* 404:604–609.

Politz, J. C., E. S. Browne, D. E. Wolf, and T. Pederson. 1998. Intranuclear diffusion and hybridization state of oligonucleotides measured by fluorescence correlation spectroscopy in living cells. *Proc. Natl. Acad. Sci.* 95:6043–6048.

Press, W., S. A. Teukolsky, W. V. Vetterling, and B. P. Flannery. 1992. Numerical Recipes in C. Cambridge University Press, Cambridge.

Rihs, H.-P., D. A. Jans, and R. Peters. 1991. The rate of nuclear cytoplasmic protein transport is determined by the casein kinase II site flanking the nuclear localization sequence of the SV40 T-antigen. *EMBO J.* 10:633–639.

Rihs, H.-P., and R. Peters. 1989. Nuclear transport kinetics depend on phosphorylation-site-containing sequences flanking the karyophilic signal of the Simian Virus 40 T-antigen. *EMBO J.* 8:1479–1484.

Saxton, M. J. 1997. Single-particle tracking: the distribution of diffusion coefficients. *Biophys. J.* 72:1744–1753.

Saxton, M. J., and K. Jacobson. 1997. Single-particle tracking: applications to membrane dynamics. *Annu. Rev. Biophys. Biomol. Struct.* 26: 373–399.

Schmidt, T., G. J. Schütz, W. Baumgartner, H. J. Gruber, and H. Schindler. 1995. Characterization of photophysics and mobility of single molecules in a fluid lipid membrane. *J. Phys. Chem.* 99:17662–17668.

Schmidt, T., G. J. Schütz, W. Baumgartner, H. J. Gruber, and H. Schindler. 1996. Imaging of single molecule diffusion. *Proc. Natl. Acad. Sci.* 93:2926–2929.

Schulz, B., and R. Peters. 1987. Nucleocytoplasmic protein traffic in single mammalian cells studied by fluorescence microphotolysis. *Biochim. Biophys. Acta.* 930:419–431.

Seksek, O., J. Biwersi, and A. S. Verkman. 1997. Translational diffusion of macromolecule-sized solutes in cytoplasm and nucleus. *J. Cell Biol.* 138:131–142.

Shelby, R. D., K. M. Hahn, and K. Sullivan. 1996. Dynamic elastic behaviour of α-satellite DNA domains visualized in situ in living human cells. *J. Cell Biol.* 135:545–557.

Smith, P. R., I. E. G. Morrison, K. M. Wilson, N. Fernández, and R. J. Cherry. 1999. Anomalous diffusion of major histocompatibility complex class I molecules on HeLa cells determined by single particle tracking. *Biophys. J.* 76:3331–3344.

Wedekind, P., U. Kubitscheck, O. Heinrich, and R. Peters. 1996. Line scanning microphotolysis for diffraction limited measurements of lateral diffusion. *Biophys. J.* 71:1621–1632.

Wedekind, P., U. Kubitscheck, and R. Peters. 1994. Scanning microphotolysis: a new photobleaching technique based on fast intensity modulation of a scanned laser beam and confocal imaging. *J. Microsc.* 176:23–33.

Weiss, S. 1999. Fluorescence spectroscopy of single biomolecules. *Science.* 283:1676–1683.

Wilson, K. M., I. E. G. Morrison, P. R. Smith, N. Fernández, and R. J. Cherry. 1996. Single particle tracking of cell-surface HLA-DR molecules using R-phycoerythrin labeled antibodies and fluorescence digital imaging. *J. Cell Sci.* 109:2101–2109.

Xie, X. S., and J. K. Trautman. 1998. Optical studies of single molecules at room temperature. *Annu. Rev. Phys. Chem.* 49:441–480.

Zhao, K., C. M. Hart, and U. K. Laemli. 1995. Visualisation of chromosomal domains with boundary element associated factor beaf-32. *Cell.* 81:879–889.

Zink, D., and T. Cremer. 1998. Cell nucleus: chromosome dynamics in nuclei of living cells. *Curr. Biol.* 8:R321–R324.

Zink, D., T. Cremer, R. Saffrich, R. Fischer, M. F. Trendelenburg, W. Ansorge, and E. H. K. Stelzer. 1998. *Hum. Genet.* 102:241–251.